

Testing for Welding, Joining or Additive Manufacturing Applications

Uğur Gürol*, Savaş Dilibal, Batuhan Turgut and Mustafa Koçak

Characterization of a low-alloy steel component produced with wire arc additive manufacturing process using metal-cored wire

<https://doi.org/10.1515/mt-2021-2155>

Abstract: In this study, a low-alloy steel component was manufactured using specially produced E70C-6M class of metal-cored welding wire according to AWS A5.18 standard for the WAAM process. The manufactured low-alloy steel component was first subjected to radiographic examination to detect any weld defect. Uniaxial tensile tests were conducted for the bottom, middle and upper regions. The micro-hardness tests were performed parallel to the deposition direction. The results show that microstructures varied from base metal to the face region of the WAAM component, including the bottom, middle and top sections. The bottom region showed lamellar structures; the middle and upper region presented equiaxed ferrite structure with a small amount of grain boundary pearlites and the face region displayed a mix of equiaxed and lamellar structures of ferrites. The yield and ultimate tensile strengths of the top, middle, and bottom regions exhibited similar results varying between 370 MPa and 490 MPa, respectively. In contrast, the top region showed an elongation value about 15% higher than other regions. Moreover, the yield and ultimate tensile strength for WAAM-produced component were found to be 14% and 24% lower than the multiple-pass all-weld metal of E70C-6M class of metal-cored wire.

Keywords: low-alloy steel; mechanical properties; metal-cored wire; microstructure; wire arc additive manufacturing.

1 Introduction

Metal additive manufacturing (MAM) has been on the rise in many industrial fields due to its relatively low cost of investment and high production speed [1, 2]. The cost of the complex shaped and larger metallic components decreases dramatically when manufactured with MAM compared to the subtractive, cast, or welded manufacturing routes. A number of metallic components can be additively manufactured using metal powder or wire materials via selective laser melting, electron beam melting, or wire arc additive manufacturing (WAAM). Among the metal additive manufacturing technologies, the robotic WAAM technology is one of the promising new manufacturing technologies provided adequate welding wire is available. Large-scale engineering components can be easily produced with high efficiency in a short production period using WAAM technology [2–5]. WAAM is also an appropriate manufacturing technology for producing the custom-made metallic components depending on the requirements in the industry. Depending on the nature of the heat source, the WAAM technology can be used in Gas Tungsten Arc Welding (GTAW), Gas Metal Arc Welding (GMAW), and Plasma Arc Welding (PAW) processes. However, the deposition rate of GMAW-based WAAM is two to three times higher than that of GTAW-based or PAW-based processes [6]. The previous studies using GMAW welding process showed that the final product, as expected, depends on the filler metal, the equipment and the process parameters used [7–11].

In WAAM-based additive manufacturing studies, the conventional solid welding wires are mainly used in the deposition process of the steel components in the literature [12–14]. Large volume of solid welding wires makes them economically feasible for commercial purpose. Thus, the commercially available welding wires of ER70S-6, ER316L and Inconel 625 are commonly preferred to perform the

*Corresponding author: Uğur Gürol, Metallurgical and Materials Engineering Department, İstanbul Gedik University, İstanbul, Turkey, E-mail: ugur.gurol@yahoo.com. <http://orcid.org/0000-0002-3205-7226>

Savaş Dilibal, Mechatronics Engineering Department, İstanbul Gedik University, İstanbul, Turkey, E-mail: savas.dilibal@gedik.edu.tr. <http://orcid.org/0000-0003-4777-7995>

Batuhan Turgut, Research and Development Center, Gedik Welding Co., İstanbul, Turkey, E-mail: bturgut@gedik.com.tr. <http://orcid.org/0000-0001-6930-2478>

Mustafa Koçak, Mechanical Engineering Department, İstanbul Gedik University, İstanbul, Turkey, E-mail: mkocak@gedik.com.tr. <http://orcid.org/0000-0001-9193-7277>

WAAM process. And also, the metallurgical properties of the deposited layers have been widely investigated in recent years. For instance, the characterization of the deposited SS316L material was examined in previous experimental studies [15]. It is known that the WAAM process parameters, as in all other welding processes, also determine the development of the final morphology of the microstructure and hence properties of the final component. Thus, recent studies [16, 17] have focused on the parametric investigations during the layer deposition process such as arc current, arc voltage, shielding gas type, welding wire feeding speed and welding wire diameter. Furthermore, the local brittle zone formation along the interface of bimetallic WAAM layers was also investigated using ER316L and ER70S-6 welding wires. The formation of the local brittle zone was attributed to the combination of Fe and C atoms along with the interface [18].

There are limited numbers of research with the WAAM using metal-cored wire [19, 20]. In the manufacturing process of the metal-cored wires, a hollow metal sheath covers the core which is filled with metallic powders of particular chemical composition which can be designed for the WAAM process. The chemical composition of metal-cored wires can be controlled to generate smooth weld layers, sufficient penetration and to avoid certain weld defects, such as crack and porosity [21]. Metal-cored welding wires are suitable for flat, vertical-down, or horizontal welds. It is known that in metal-cored wires, the electric current is conducted mainly via metallic sheath throughout the weld cycle and hence lower energy is generally needed for the metal-cored wires to melt the metallic powders compared to the same volume of the solid welding wires. Thus, the heat input in the WAAM component can be decreased when the metal-cored wires are used. Additionally, the significant advantage of metal-cored wire WAAM technology is the adjustability in the wire chemical composition to obtain high deposition efficiency for the required microstructural and mechanical characteristics of the component [22, 23]. As the growth of

WAAM-based applications in industry continue to rise, the need for the specially developed advanced welding consumables for the WAAM applications will increase in the market. A special metal-cored welding wire composition with small batches is currently manufactured at the Gedik Welding for the purpose of trials and investigations.

The microstructure and mechanical properties of XC-45 metal-cored wire for the WAAM parts were investigated by comparing with the part produced via traditional casting, forging and cold rolling process [19] and uniform hardness and comparable tensile strength were obtained. In another study [20], the WAAM performance of metal-cored Mn-steel welding wires was compared with the solid wires using the gas metal arc welding (GMAW) process under cold metal transfer (CMT) and CMT pulse control. The feasibility of the Mn-steel-based metal-cored wires for WAAM process has been experimentally confirmed. In the present study, E70C-6M class of metal-cored welding wire with the AWS A5.18 standard metal-cored wire was manufactured to be used in WAAM process. The WAAM-produced low-alloy steel component was first subjected to radiographic examination, then tensile tests were carried out with the extracted samples through the building direction in order to determine its mechanical properties. The hardness distribution along the building direction was also conducted together with the examination of the microstructural features between the layers.

2 Experimental approach

The mechanical properties of the GeKa Elcor M70 metal-cored wire was determined using the all-weld test procedures specified in AWS 5.18 standard. The all-weld tensile samples extracted from the weld plates which was welded in flat position using all-weld test assembly, Figure 1. The following process parameters was utilized through the welding process: the arc current of 280 A with the voltage of 35 V and welding speed of 40 cm/min under

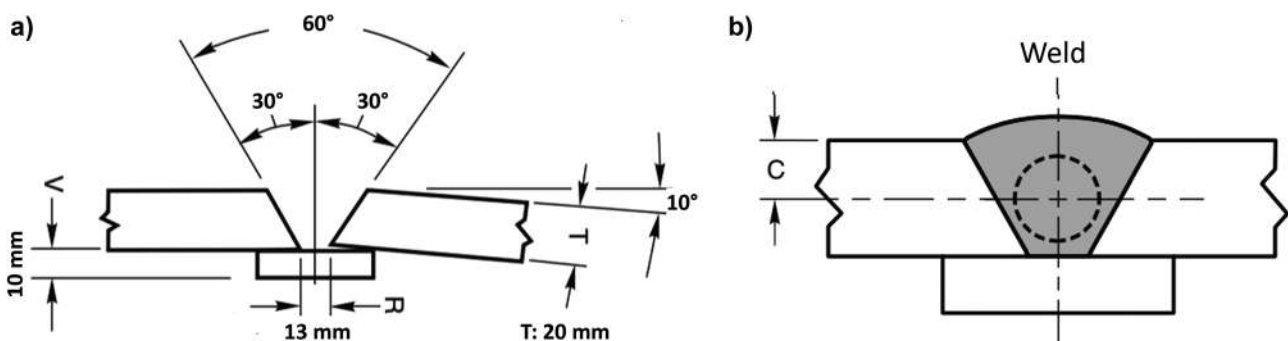


Figure 1: All-weld joint details, a) groove preparation, b) location of the tensile specimens [24].

the 82% Ar + 18% CO₂ mixture of shielding gas atmosphere using the flow rate of 15 l min⁻¹.

The main experimental setup which was employed in the WAAM process was depicted in Figure 2. The GeKa-Tec WB 500L machine with a water-cooled torch integrated on a 6-axis OTC Daihen FD-V8L robot was operated as the power source of WAAM system. The metal-cored welding wire of E70C-6 with AWS A5.18 was used as a filler metal. The rolled structural steel S355J-N with the dimensions of 350 × 300 × 12 mm³ was used as the base plate. The selected base plate was clamped to the working table before the welding process to minimize the potential distortion due to the thermal input.

The manufactured WAAM component, shown in Figure 3, was built using low spatter process. The process parameters used are shown in Table 1. It is known [16] that the inter-layer cooling time directly influences the temperature distribution of the thin-walled body as manufactured in this study, hence the inter-layer temperature was measured before deposition of the next layer using the infrared thermometer. The weld layers continuously deposited by keeping the inter-pass temperature and timing constant till the component is fully completed, as shown in Figure 3. The measured inter-pass temperature

fluctuates in the temperature range of 140–340 °C during the deposition process.

To detect any defects which may be present in the manufactured component, X-ray radiographic test (RT) was conducted. Upon completion of the X-ray testing, tensile test specimens were extracted according to the ASTM E8/E8M-21 from the straight wall parts, as shown in the Figures 3b–d.

Standard steel grinding and polishing procedures for the cross-sectional surface were applied utilizing an Abramin Struers auto-grinder/polisher followed by etching using 3 wt% Nital as the reagent. To investigate mechanical properties of the deposited wall through the tensile tests, three samples were extracted along the building direction. The microstructural characterization along the building direction was conducted using the Leica DMi8 optical microscope. Furthermore, Vickers hardness tests were made using Struers DuraScan G5 in the transversal section of the component in order to analyze the hardness of the extracted samples. The ARL OES 8860 optical emission spectrometer was utilized to perform chemical analyses of the cross-sectional samples both WAAM component and all-weld test plate.



Figure 2: The experimental setup used for the wire arc additive manufacturing process.

3 Results and discussion

The macrograph of the multi-pass welding of the all-weld test plate is shown in Figure 4. The columnar and recrystallized (reheated) zones are the main weld metal regions of the multi-pass welding process and hence large portion of the all-weld metal contains reheated zones except for the last bead. Hence, the central part of the weld metal used for the tensile test specimen represent the reheated weld metal. The effect of multi-pass welding on the low alloyed steel welds are complex due to the existence of columnar and reheated (with refined grains) microstructures where these regions differ with welding process parameters such as inter-pass temperature, heat input and chemical composition [25]. Figure 5a revealed that the columnar zone has a mixture of acicular ferrite (AF), grain boundary ferrite (GBF) and Widmanstätten ferrite (WF). In contrast, polygonal ferrite (PF) with small fraction of pearlite (P) were formed in the reheated zone (Figure 5b). It is well known that the presence of finer grain AF microstructure in the weld metal deposit, would improve its strength and toughness, thereby ensuring good mechanical properties [26]. This is due to the fine grain microstructure acts effective barrier against crack growth and hence increases the fracture toughness [27].

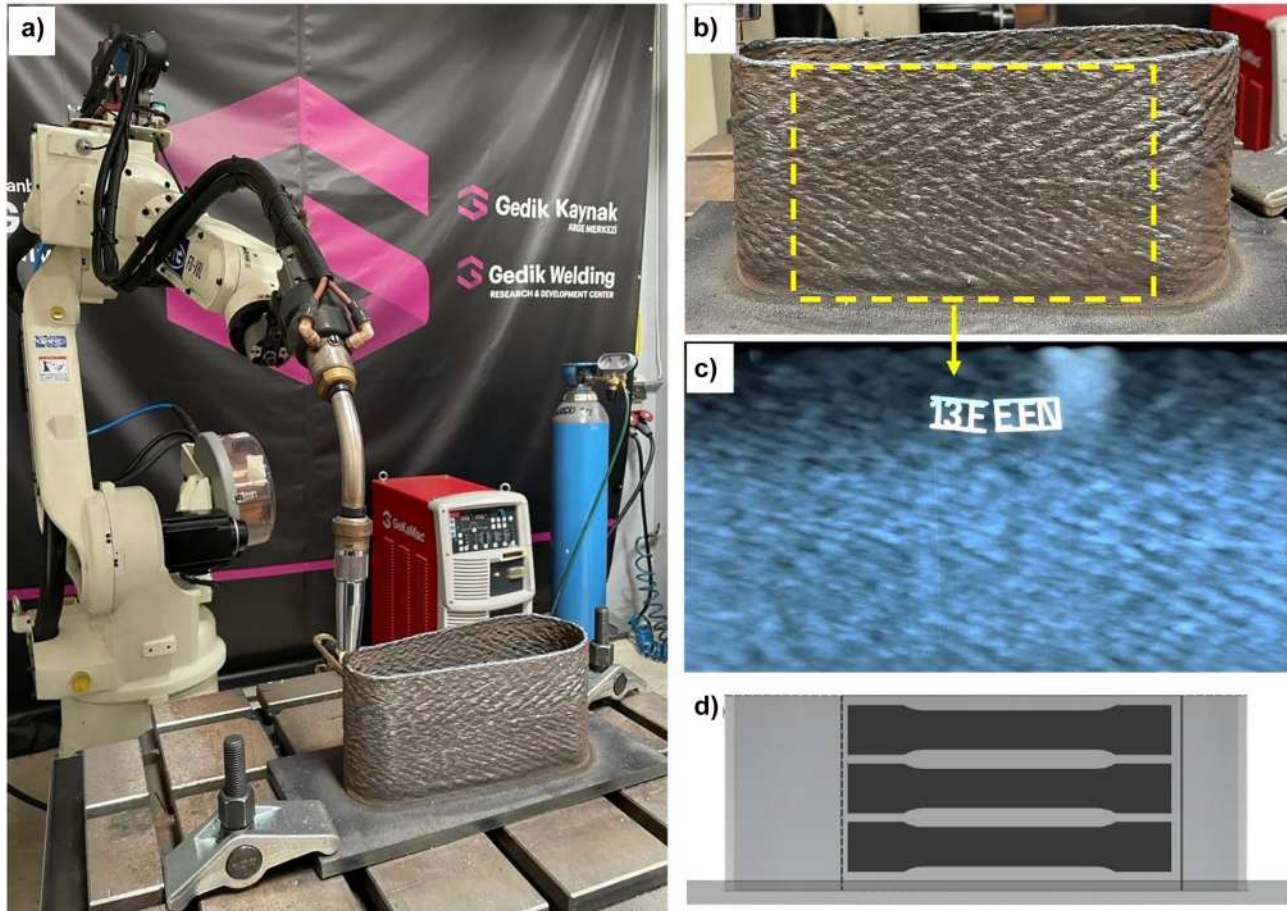


Figure 3: The details of the WAAM produced component, a) general view, b) radiographic test location shown in yellow rectangle, c) radiographic test results, d) location of the tensile samples.

Table 1: The process parameters.

Parameters	Unit	E70C-6M
Voltage	V	15
Current	A	70
Wire diameter	mm	1.2
Welding speed	cm min ⁻¹	40
Torch angle	degree	90°
Shielding gas type	–	82% Ar + 18% CO ₂
Gas flow rate	l min ⁻¹	15

The chemical compositions of the E70C-6M all-weld metal and WAAM component are presented in Table 2 and showed that both weld depositions have the same chemical compositions since the same welding wire was used in both welds.

The macrostructure of the single bead wall of WAAM weld deposit composed of hundred layers is shown in Figure 6. There are no major defects such as cracks, slag,

and porosity in both in the welded layers and the interface zones of the deposited walls. Detailed examination of the WAAM part showed the fully and continuously metallurgically integrated layer depositions. This indicates that the consumable E70C-6M metal-cored welding wire is fully compatible for WAAM-based deposition process. In addition, the inter-pass temperature becomes higher with the deposition of each layer. During the deposition of the first 10–15 layers, the inter-pass temperature increased rapidly, then showed slow increase then gradually reached a constant value (of about 300 °C) after 70th layers. The results of the measured temperature curves somehow correlate with the microstructural analysis of the zones, as well as with the hardness and tensile tests.

The overall microstructures of the E70C-6M steel WAAM wall at different regions along the building direction including base metal (Area A), fusion boundary (Area B), bottom (Area C), middle region, (Area D), upper region (Area E) and face region (Area F) were demonstrated with optical micrographs in Figures 7–12. The microstructure of

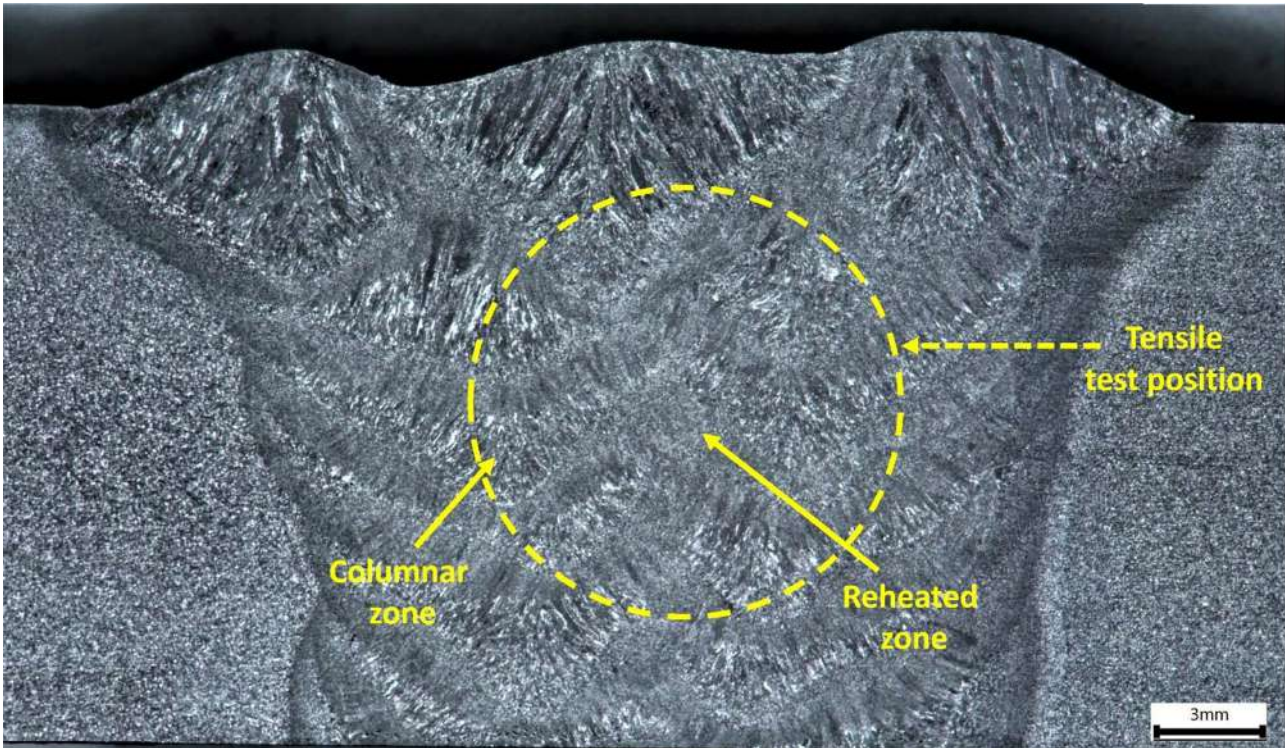


Figure 4: Macro view of the all-weld metal showing the columnar and reheated zones as well as round tensile specimen location.

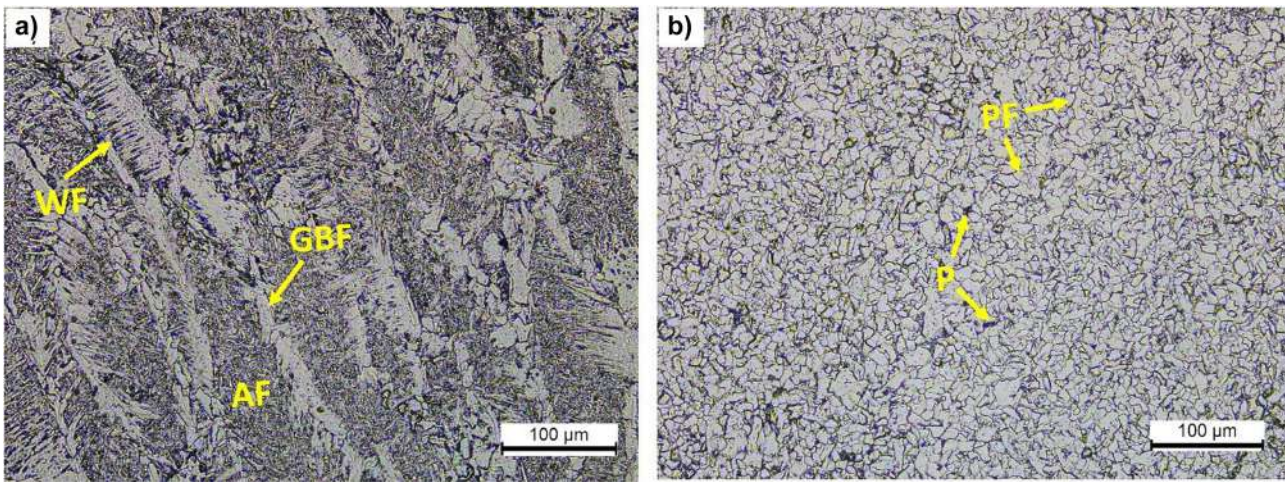


Figure 5: Microstructure of the all-weld metal, a) columnar zone, b) reheated zone.

Table 2: Chemical compositions of the all-weld metal and WAAM-produced component (wt%).

	C	Si	Mn	P	S
E70C-6M acc. AWS	Max.	Max.	Max.	Max.	Max.
A5.18	0.12	0.90	1.75	0.03	0.03
All-weld metal	0.051	0.55	1.19	0.022	0.008
WAAM component	0.050	0.55	1.12	0.021	0.008

the substrate S355J-N steel presents a regular ferrite matrix (white) with a secondary pearlite phase (black islands) as shown in Figure 7.

Figure 7 shows optical micrographs near the interface between the E70C-6M filler metal and S355J-N base metal. No process defects (pores, cracks, or delineations) were observed along the interface which indicates good metallurgical bonding. The E70C-6M side of the interface showed

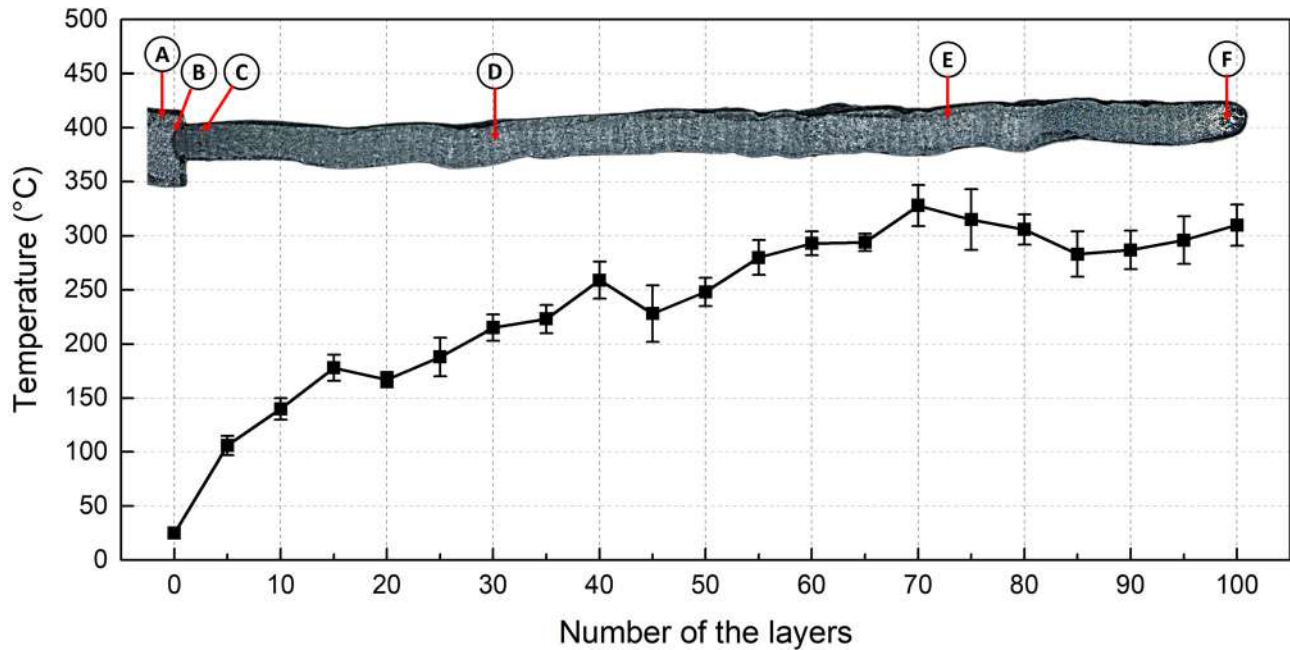


Figure 6: The measured inter-pass temperature values with increase of welding layers.

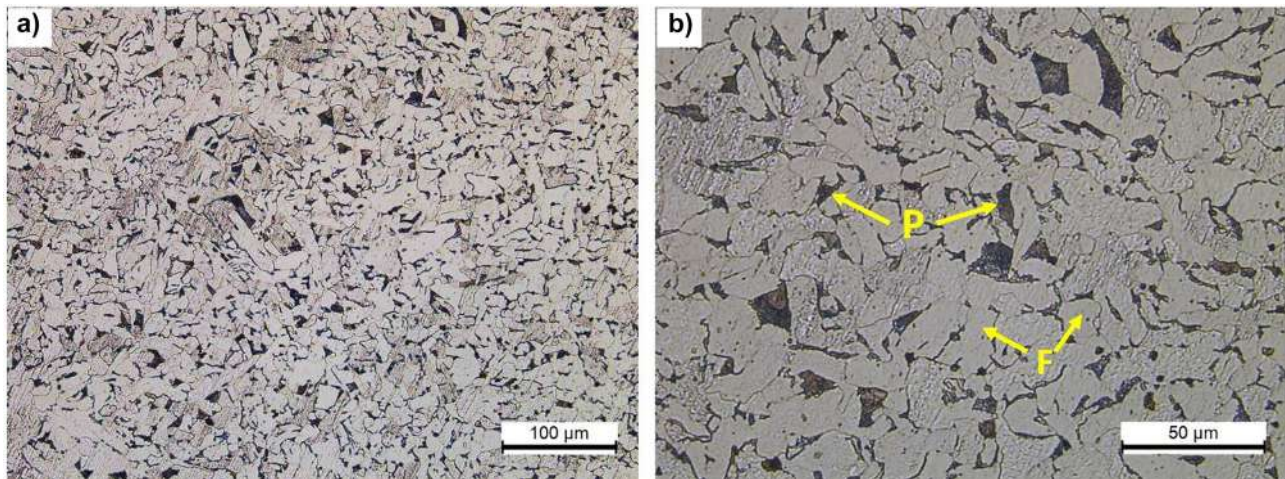


Figure 7: Optical micrographs taken from region A (base metal) depicted of the temperature variation diagram in Figure 6.

the formation of lamellar structures composed some nonequilibrium phases such as AF, GBF and WF adjacent to the melt-pool boundary due to the faster cooling that was mainly caused by the substrate plate. The bottom region after 2–3 passes from the interface also was affected by the cooler substrate plate and hence caused a higher cooling rate during the solidification and the microstructure is showing the formation of AF, GBF and WF features in Figure 8. The formation of the WF at the bottom region can be caused from the migration of carbon atoms to the center as reported in [28].

It is also reported in [19] that the heat accumulation increases in the middle region with the increased building layers. Because, in these regions, cooling, besides convection and radiation, which was similar for all layers, was governed by conduction throughout the already deposited layers. Hence, the middle region presents a lower thermal gradient with lower cooling rate compared to the bottom region [20]. This occurs due to the influence of continuous cooling with air and the heat conduction through the bottom of the built sample. Therefore, the width of the columnar zone diminished with the increasing number of

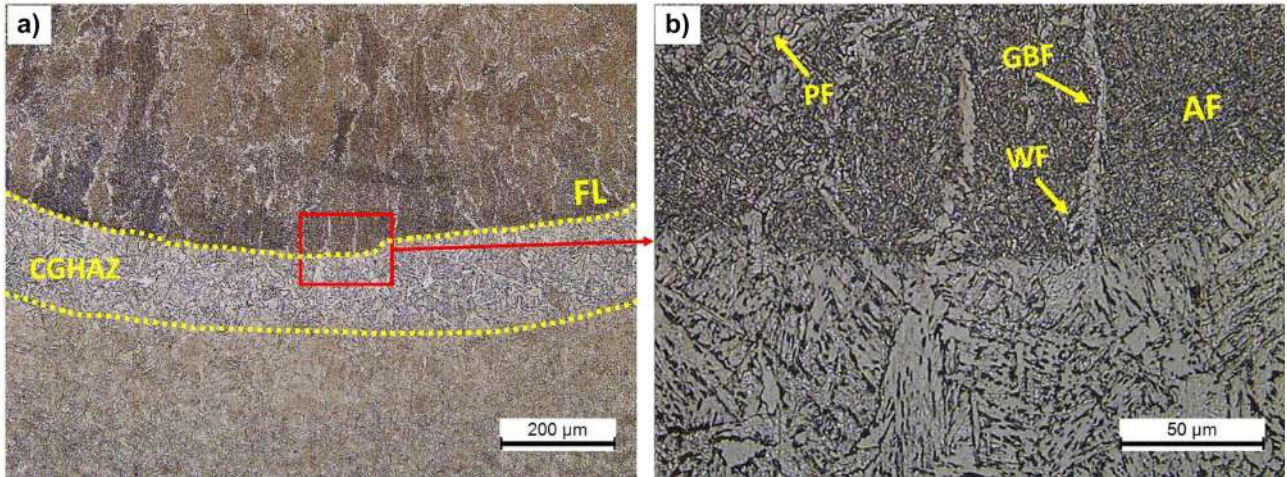


Figure 8: Optical micrographs taken from the region B depicted on the temperature variation diagram in Figure 6.

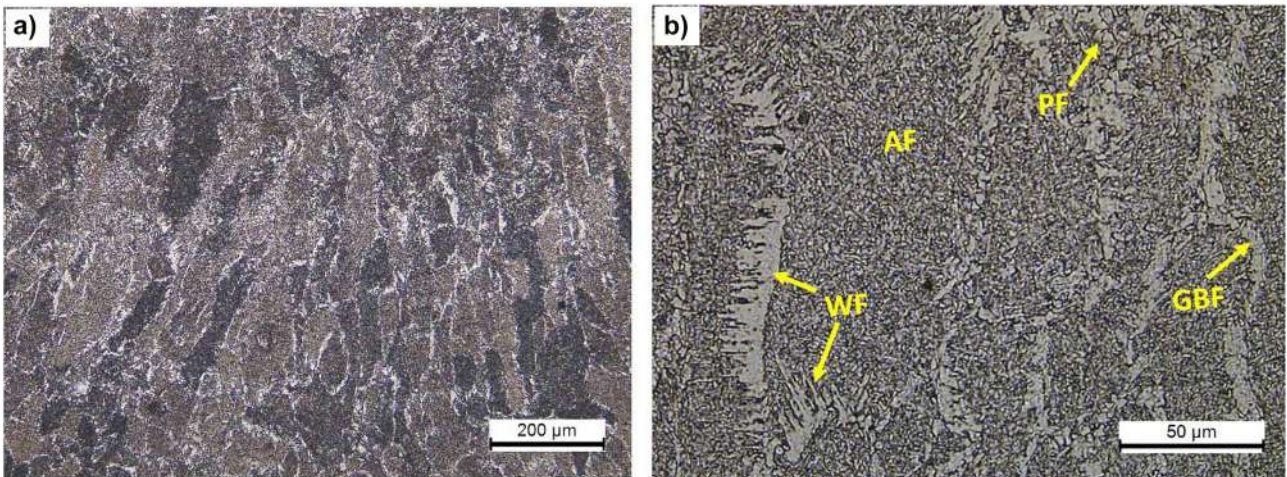


Figure 9: Optical micrographs taken from region C depicted on the temperature variation diagram in Figure 6.

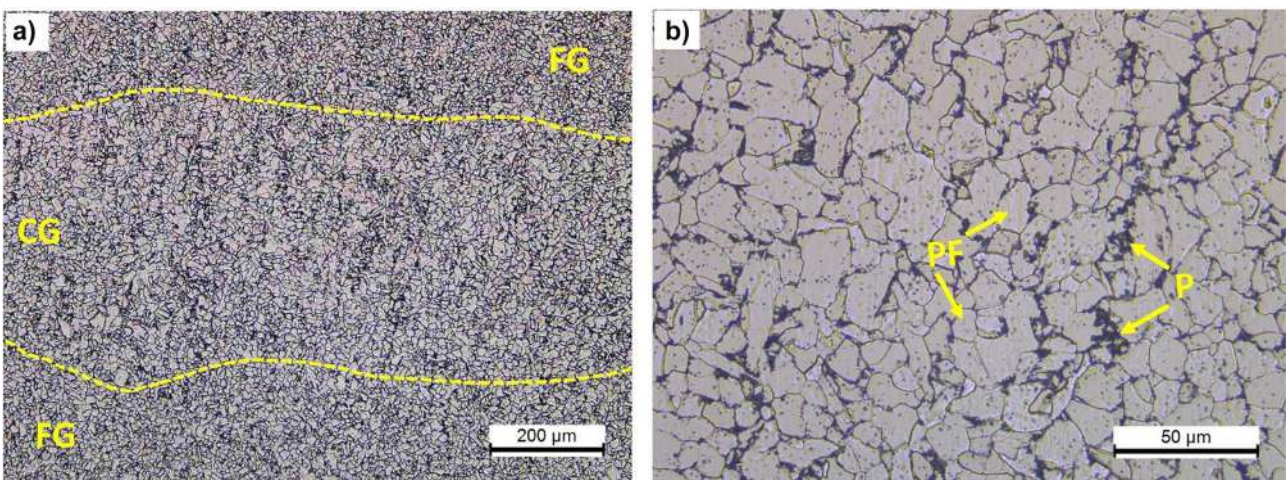


Figure 10: Optical micrographs taken from the region D depicted on the temperature variation diagram in Figure 6.

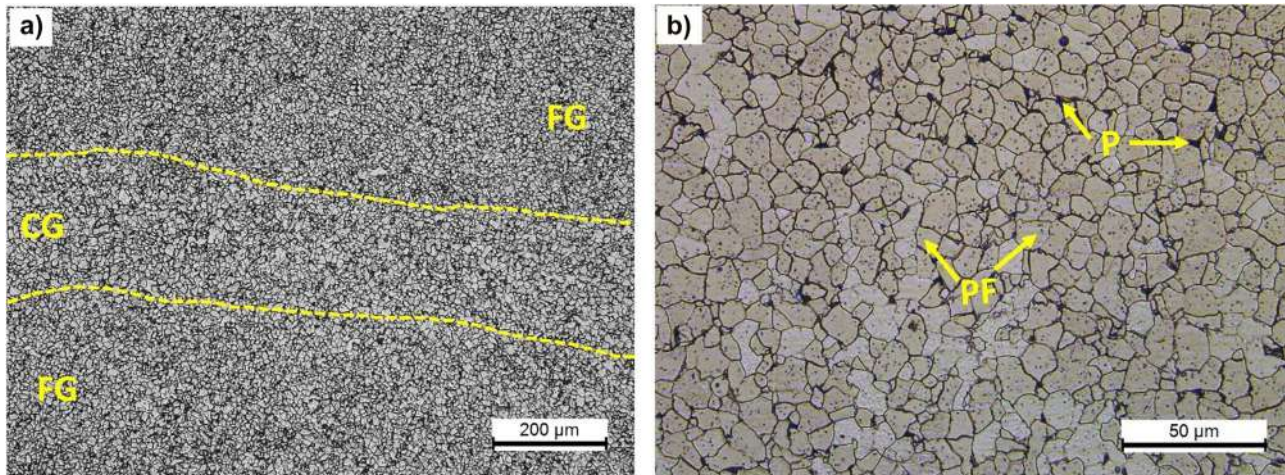


Figure 11: Optical micrographs taken from the region E depicted on the temperature variation diagram in Figure 6.

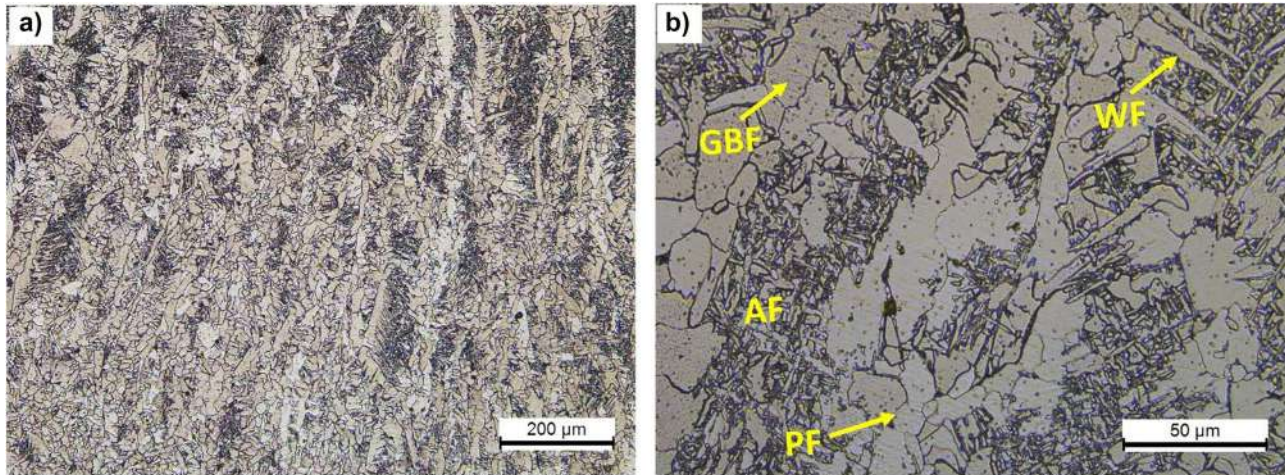


Figure 12: Optical micrographs taken from the region F depicted on the temperature variation diagram in Figure 6.

layers. The microstructures of middle and upper regions were found to be having more polygonal and quasi-polygonal structures of ferrite with a small amount of pearlite at the grain boundaries and some variation in grain size as shown in Figures 10 and 11. No dendritic structure was found in both regions due to the continuous recrystallization. Similar results were reported in a previous study for low-carbon low-alloy steel fabricated by WAAM process [14, 29]. Moreover, it was also found two types of microstructures in these both regions as shown in Figures 10 and 11. The relatively smaller ferrite grains were found in the center of melt pool and the coarse grains were generated in the heat-affected zone of the previously deposited WAAM layer. This is a direct consequence of the grain boundaries migration in the previously deposited

layer, triggered by the significantly high temperature from deposition of a new layer. To compare both regions, the widths of the coarse-grained (CG) and fine grained (FG) regions were measured in vertical mid-plane position. The width of the coarse-grained area was found to be lower in upper region compared to middle region. This could be attributed to increasing inter-pass temperature along the wall direction.

The face region (Area F) consists of the finally deposited layer and shows higher cooling rate because of the contact with the open air at room temperature (Figure 12). Thus, its microstructure forms with a mix of the lamellar and equiaxed structures of ferrites which composed of PF, WF, GBF and AF. Higher cooling rate caused a transformation of microstructures from the primary austenite

dendrites into typical WF microstructure [12]. Such formation of AF, WF and GBF of the face region was also reported in previous studies during wire arc additive manufacturing of low-carbon low-alloy steels [30–32]. Moreover, it is clearly visible that the grain size of the B which is next to fusion line (FL) is finer than that of the F region since the B contacts the cold substrate at room-temperature while the F region contacts warm deposited layers. Similar micrographic results found in the literature as in Ref [14].

The stress-strain curves for the Top-L, Middle-L, and Bottom-L longitudinal samples extracted from the as-built WAAM component and all-weld tensile results of E70C-6M wire are given in Figure 13. The all-weld metal deposited with E70C-6M wire showed yield strength of 479 MPa, an ultimate tensile strength of 559 MPa and an elongation to fracture of 25.6%. The tensile samples extracted from bottom, middle and top locations of the WAAM part showed average yield strength of 370 MPa and tensile strength of 490 MPa in the deposition direction, Figure 13. However, the top showed an elongation value about 15% more than bottom and middle region. The increment of refined grains increased the value of elongation at the top region (Figures 9 and 10). On the other hand, the ultimate tensile strength and yield strength dramatically decreased with the value of 14% and 24% in the deposition direction, respectively, in comparison with the all-weld metal deposit. This can be attributed to the AF generated microstructure refinement in the all-weld metal deposit compared to the WAAM-built component.

Figure 14 shows hardness distribution of all-weld metal taken from the tensile test location. It was found that

reheated zone between the passes showed the lower hardness values compared the columnar zones (L1 and L3 of Figure 14). Because the preceding columnar morphology is changed to mainly polygonal ferrite and led to the refinement of the microstructure in the reheating process, this tempering effect decreased the weld metal hardness [27]. These hardness results once more show the development of lower strength (Figure 13) WAAM component (Figure 15).

The microhardness characteristics of the extracted WAAM samples at multiple points were shown in Figure 14. The base metal showed the lowest hardness value due to the coarse ferrite grains as shown in Figure 6. The region C which is located at the first deposits along the substrate revealed the highest hardness value due to WF microstructures with the fine AF formation as shown in Figure 9. Additionally, the face region (region F) has higher microhardness values than that of the middle and upper region due to the presence of lamellar structures as shown in Figure 12. On the other hand, the hardness values of WAAM component, especially in region D and E showed lower hardness values than all-weld metal of E70C-6M metal-cored wire.

The microstructure of the final component depends on the thermal history through the manufacturing process. The particular WAAM thermal cycle, which involves repeated heat cycles and subsequently cooling produces lower hardness (about 150 HV) reheated finer and uniform microstructure the fabricated component. It has shown that the identical welding wire produced weld metal in WAAM-produced component which is different than the conventional butt-joint type weld metal. The WAAM-produced component has

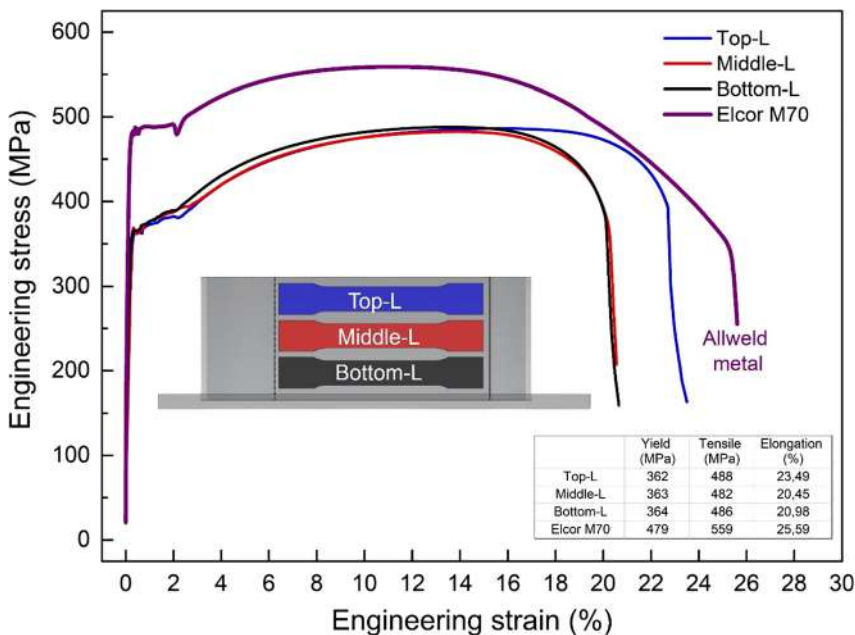


Figure 13: The stress-strain curves for the top-L, middle-L, and bottom-L horizontal samples of the component and comparison with the stress-strain curve of the all-weld metal.

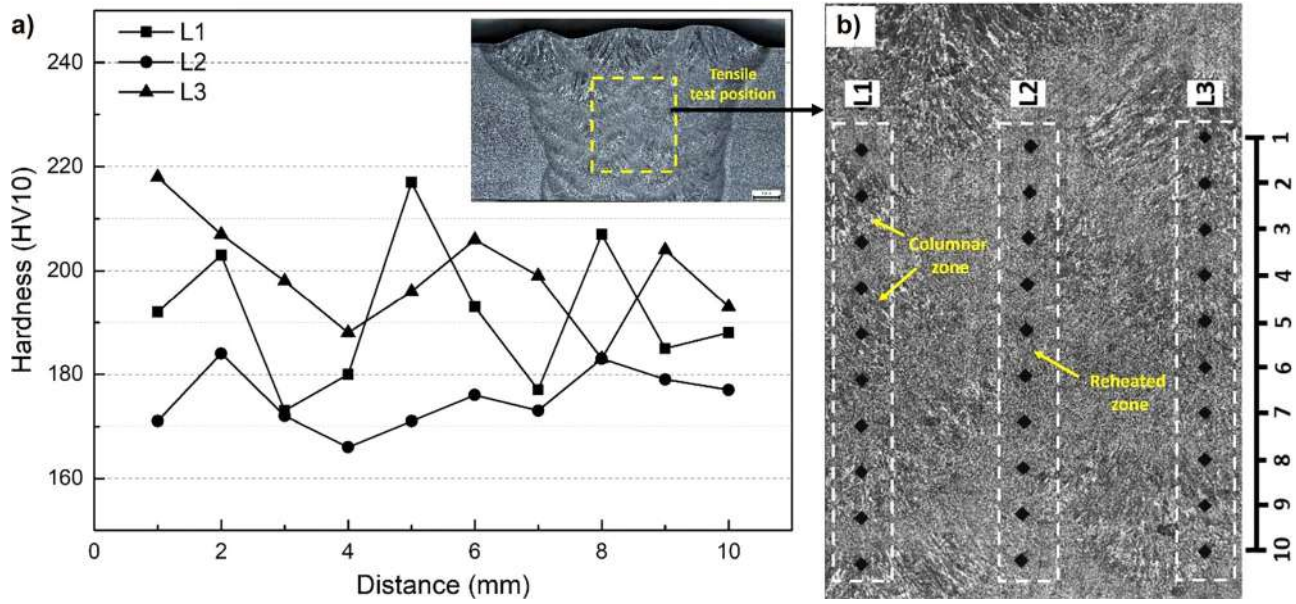


Figure 14: Hardness distribution of the all-weld metal, a) test results, b) test locations showing columnar and reheated zones.

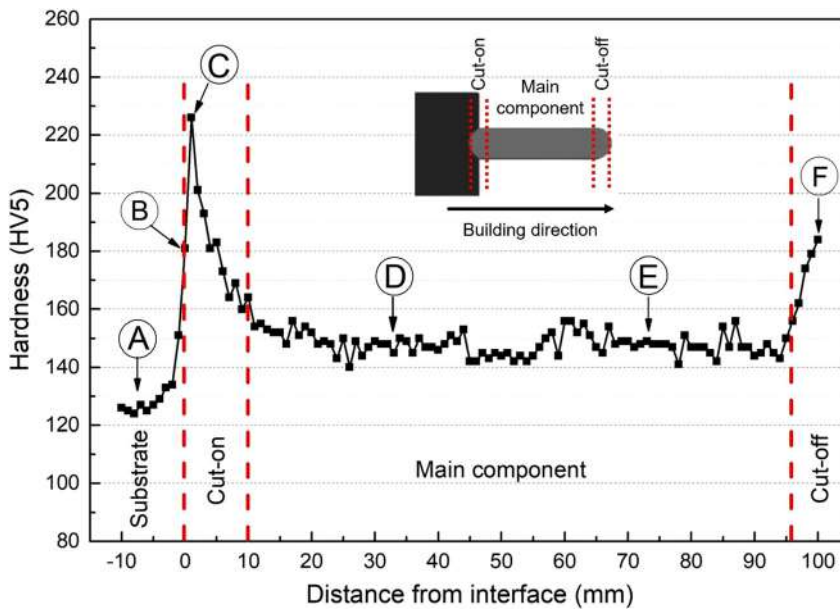


Figure 15: Hardness distribution of the WAAM-produced component along the building direction.

lower yield and ultimate tensile strength than the all-weld-metal produced for joining of the plates as shown in Figure 13. Similarly, Nagasai et al. [33] also reported that the tensile properties of cylinder wall produced using ER70S-6 solid wire are also lower than the filler metal (all-weld metal). These results are important to remind the designers that demonstrated mechanical properties of the present welding wires manufactured for the joining of the materials can be used after the optimization of the heat input and cooling rate for the additive manufacturing process. This study revealed that WAAM components show lower tensile properties than

filler metal due to the continuously deposition resulting the considerable heat input and severe damage to the previously deposited layers.

4 Conclusions

In this study, the E70C-6M class of metal-cored wire was used in the robotic wire arc additive manufacturing process. The microstructure and mechanical characteristics of the as-deposited low-alloy steel component were investigated and

compared with the mechanical properties of the all-weld metal made of the same welding wire. The main objective of the study was to demonstrate the feasibility of the E70C-6M class of metal-cored welding wire in robotic WAAM applications.

The obtained results were summarized as below.

- The E70C-6M metal-cored wire can be used successfully to produce low-alloy steel components by WAAM without any significant defects such as lack of penetration, pores, or cracks.
- The detailed metallographic investigations of the microstructure of the as-deposited thin-walled component showed that the microstructure varies from the base metal to the face regions since the regions experience different thermal heat cycles and cooling conditions during the continuous manufacturing process of the subsequent layers. The local microstructural characteristics leads to the variation in hardness in each region while having main part with similar tensile properties. However, the top region showed an elongation value about 15% more than the bottom and middle region due to higher number of fine-grained areas in upper region.
- The yield and ultimate tensile strength of the WAAM part were found to be 14% and 24% lower than the all-weld metal produced in multi-pass butt-joint, respectively. The reduced strength of the component was associated with presence of higher volume fraction of reheated regions resulting in decrease in lamellar structure with acicular ferrite. The designer of the metallic parts should pay attention to this matter, if single layer WAAM process is going to be used by using commercially available E70C-6M metal-cored wire for the manufacturing of the steel part.

In the future work, the effect of heat input and cooling rate of WAAM-produced material will be investigated using both sub-sized Charpy and tensile specimens to generate the input data for the designers of the industrial steel components produced via WAAM process.

Acknowledgments: Authors wish to acknowledge the valuable contributions of Ms. Nurten Güleçyüz for assisting the robotic welding and the WAAM operations.

Author contribution: All the authors have accepted responsibility for the entire content of this submitted manuscript and approved submission.

Research funding: None declared.

Conflict of interest statement: The authors declare no conflicts of interest regarding this article.

References

- [1] W. E. Frazier, “Metal additive manufacturing: a review,” *J. Mater. Eng. Perform.*, vol. 23, pp. 1917–1928, 2014, <https://doi.org/10.1007/s11665-014-0958-z>.
- [2] G. Çam, “Prospects of producing aluminum parts by wire arc additive manufacturing (WAAM),” *Mater. Today: Proc.*, 2022, <https://doi.org/10.1016/j.matpr.2022.02.137>.
- [3] J. Xiong, Y. Li, R. Li, and Z. Yin, “Influences of process parameters on surface roughness of multi-layer single-pass thin-walled parts in GMAW-based additive manufacturing,” *J. Mater. Process. Technol.*, vol. 252, pp. 128–136, 2018, <https://doi.org/10.1016/j.jmatprotec.2017.09.020>.
- [4] G. Chun, L. Maoxue, H. Ruizhang, et al., “High-strength wire + arc additive manufactured steel,” *Int. J. Mater. Res.*, vol. 111, no. 4, pp. 325–331, 2020, <https://doi.org/10.3139/146.111890>.
- [5] H. Chaoyu, C. Zhipeng, F. Manjie, et al., “Microstructure characterization of SAW and TIG welded 25Cr2Ni2MoV rotor steel metal,” *Metals*, vol. 10, Art no. 603, 2020. <https://doi.org/10.3390/met10050603>.
- [6] W. Bintao, Z. Pan, D. Ding, et al., “A review of the wire arc additive manufacturing of metals: properties, defects and quality improvement,” *J. Manuf. Process.*, vol. 35, pp. 127–139, 2018, <https://doi.org/10.1016/j.jmapro.2018.08.001>.
- [7] K. S. Derekar, A. Addison, S. S. Joshi, et al., “Effect of pulsed metal inert gas (pulsed-MIG) and cold metal transfer (CMT) techniques on hydrogen dissolution in wire arc additive manufacturing (WAAM) of aluminium,” *Int. J. Adv. Manuf. Techn.*, vol. 107, pp. 311–331, 2020, <https://doi.org/10.1007/s00170-020-04946-2>.
- [8] J. Xiong and G. Zhang, “Adaptive control of deposited height in GMAW-based layer additive manufacturing,” *J. Mater. Process. Technol.*, vol. 214, no. 4, pp. 962–968, 2014, <https://doi.org/10.1016/j.jmatprotec.2013.11.014>.
- [9] D. H. Ding, Z. X. Pan, C. Dominic, and H. J. Li, “Process planning strategy for wire and arc additive manufacturing,” in *Robotic Welding, Intelligence and Automation RWIA Advances in Intelligent Systems and Computing*, vol. 363, T. J. Tarn, S. B. Chen, and X. Q. Chen, Eds., 2015, pp. 437–450.
- [10] J. Xiong, Y. Lei, H. Chen, and G. Zhang, “Fabrication of inclined thin-walled parts in multilayer single pass GMAW based additive manufacturing with flat position deposition,” *J. Mater. Process. Technol.*, vol. 240, pp. 397–403, 2017, <https://doi.org/10.1016/j.jmatprotec.2016.10.019>.
- [11] B. Wittig, M. Zinke, and S. Jüttner, “Influence of arc energy and filler metal composition on the microstructure in wire arc additive manufacturing of duplex stainless steels,” *Weld. World*, vol. 65, pp. 47–56, 2021, <https://doi.org/10.1007/s40194-020-00995-z>.
- [12] V. T. Le, D. S. Mai, and Q. H. Hoang, “A study on wire and arc additive manufacturing of low carbon steel components: process stability, microstructural and mechanical properties,” *J. Braz. Soc. Mech. Sci. Eng.*, vol. 42, 2020, Art no. 480, <https://doi.org/10.1007/s40430-020-02567-0>.
- [13] V. T. Le, T. L. Banh, D. T. Nguyen, and V. T. Le, “Wire arc additive manufacturing of thin-wall low-carbon steel parts: microstructure and mechanical properties,” *Int. J. Mod. Phys. B*,

- vol. 34, no. 22n24, 2020, Art no. 204015, <https://doi.org/10.1142/S0217979220401542>.
- [14] M. Rafieazad, M. Ghaffari, A. V. Nemani, and A. Nasiri, “Microstructural evolution and mechanical properties of a low-carbon low-alloy steel produced by wire arc additive manufacturing,” *Int. J. Adv. Manuf.*, vol. 105, pp. 2121–2134, 2019, <https://doi.org/10.1007/s00170-019-04393-8>.
- [15] X. Chen, J. Li, X. Cheng, et al., “Microstructure and mechanical properties of the austenitic stainless steel 316L fabricated by gas metal arc additive manufacturing,” *Mater. Sci. Eng. A*, vol. 703, pp. 567–577, 2017, <https://doi.org/10.1016/j.msea.2017.05.024>.
- [16] A. Waqas, X. Qin, J. Xiong, H. Wang, and C. Zheng, “Optimization of process parameters to improve the effective area of deposition in GMAW-based additive manufacturing and its mechanical and microstructural analysis,” *Metals*, vol. 9, p. 775, 2019, <https://doi.org/10.3390/met9070775>.
- [17] D. Yang, G. Wang, and G. Zhang, “Thermal analysis for single-pass multi-layer GMAW based additive manufacturing using infrared thermography,” *J. Mater. Process. Technol.*, vol. 244, pp. 215–224, 2017, <https://doi.org/10.1016/j.jmatprotec.2017.01.024>.
- [18] U. Gürol, B. Turgut, N. Gülecüyüz, S. Dilibal, and M. Kocak, “Development of multi-material components via robotic wire arc additive manufacturing,” *Int. J. 3D Printing Technol. Digital Ind.*, vol. 5, no. 3, pp. 721–729, 2021, <https://doi.org/10.46519/ij3dptdi.1033374>.
- [19] Z. Lin, C. Goulas, W. Ya, and M. J. M. Hermans, “Microstructure and mechanical properties of medium Carbon steel deposits obtained via wire and arc additive manufacturing using metal-cored wire,” *Metals*, vol. 9, 2019, Art no. 673, <https://doi.org/10.3390/met9060673>.
- [20] P. C. Jaeger Rocha, “Metal-cored wire + arc additive manufacturing of thick layered structures with GMAW process,” Master thesis, Florianópolis, Brazil, Universidade Federal de Santa Catarina, 2020, [online]. Available at: <https://repositorio.ufsc.br/handle/123456789/220409> [accessed March 27, 2021].
- [21] J. Yu and S. M. Cho, “Metal-cored welding wire for minimizing weld porosity of zinc-coated steel,” *J. Mater. Proc. Technol.*, vol. 249, pp. 350–357, 2017, <https://doi.org/10.1016/j.jmatprotec.2017.06.012>.
- [22] B. Arivazhagan and M. Kamaraj, “Metal-cored arc welding process for joining of modified 9Cr-1Mo (P91) steel,” *J. Manuf. Process.*, vol. 15, no. 4, pp. 542–548, 2013, <https://doi.org/10.1016/j.jmapro.2013.07.001>.
- [23] B. Wu, Z. Pan, D. Ding, et al., “A review of the wire arc additive manufacturing of metals: properties, defects and quality improvement,” *J. Manuf. Process.*, vol. 35, pp. 127–139, 2018, <https://doi.org/10.1016/j.jmapro.2018.08.001>.
- [24] AWS A5 Committee on Filler Metals and Allied Materials, “Specification for carbon steel electrodes and rods for gas shielded arc welding,” in *AWS A5.18/A5.18M*, 8th ed. Miami, American Welding Society, 2021.
- [25] Y. Kang, K. Han, J. Park, and C. Lee, “Variation in the chemical driving force for intragranular nucleation in the multi-pass weld metal of Ti-containing high strength low-alloy steel,” *Metall. Mater. Trans.: Phys Metall. Mater. Sci., A*, vol. 46, no. 8, pp. 3581–3591, 2015, <https://doi.org/10.1007/s11661-015-2958-5>.
- [26] Y. Dai, S. Yu, A. Huang, and Y. Shi, “Microstructure and mechanical properties of high-strength low alloy steel by wire and arc additive manufacturing,” *Int. J. Miner. Metall.*, vol. 27, pp. 933–942, 2020, <https://doi.org/10.1007/s12613-019-1919-1>.
- [27] J. C. F. Jorge, L. F. G. Souza, M. C. Mendes, et al., “Microstructure characterization and its relationship with impact toughness of C-Mn and high strength low alloy steel weld metals – a review,” *J. Mater. Res. Technol.*, vol. 10, pp. 471–501, 2021, <https://doi.org/10.1016/j.jmrt.2020.12.006>.
- [28] M. R. U. Ahsan, A. N. M. Tanvir, G. Seo, et al., “Heat-treatment effects on a bimetallic additively-manufactured structure (BAMS) of the low-carbon steel and austenitic-stainless steel,” *Addit. Manuf.*, vol. 32, 2020, Art no. 101036, <https://doi.org/10.1016/j.addma.2020.101036>.
- [29] M. Rafieazad, A. V. Nemani, M. Ghaffari, and A. Nasiri, “On microstructure and mechanical properties of a low-carbon low-alloy steel block fabricated by wire arc additive manufacturing,” *J. Mater. Eng. Perform.*, vol. 30, no. 7, pp. 4937–4945, 2021, <https://doi.org/10.1007/s11665-021-05568-9>.
- [30] U. Reisgen, R. Sharma, S. Mann, and L. Oster, “Increasing the manufacturing efficiency of WAAM by advanced cooling strategies,” *Weld. World*, vol. 64, no. 64, pp. 1409–1416, 2020, <https://doi.org/10.1007/s40194-020-00930-2>.
- [31] V. T. Le and H. Paris, “On the use of gas-metal-arc-welding additive manufacturing for repurposing of low-carbon steel components: microstructures and mechanical properties,” *Weld. World*, vol. 65, pp. 157–166, 2021, <https://doi.org/10.1007/s40194-020-01005-y>.
- [32] L. Jingchuan, Y. Guoqiang, L. Dashi, Z. Sheng, P. Lizhen, and Q. Liu, “Effect of modified water-bath method on microstructure and mechanical properties of wire arc additive manufactured low-carbon low-alloy steel,” *Steel Res. Int.*, vol. 92, no. 4, 2021, Art no. 2000523, <https://doi.org/10.1002/srin.202000523>.
- [33] N. B. Prasanna, S. Malarvizhi, and V. Balasubramanian, “Mechanical properties of wire arc additive manufactured carbon steel cylindrical component made by gas metal arc welding process,” *J. Mech. Behav. Mater.*, vol. 30, no. 1, pp. 188–198, 2021, <https://doi.org/10.1515/jmbm-2021-0019>.

The authors of this contribution

Uğur Gürol

Assistant Prof. Dr. Uğur Gürol, born in 1989, graduated with a PhD degree (2020) in Metallurgical & Materials Engineering from Sakarya University, Turkey. He is currently working as an academic member of Istanbul Gedik University, and R&D Manager of Gedik Welding Inc. He is also CEO of Turkish Authorized National Body of Additive Manufacturing (EWF TR AM ANB). His main research areas are welding metallurgy, steel casting and additive manufacturing.

Savaş Dilibal

Associate Prof. Dr. Savaş Dilibal, received his BS in System Engineering from the Army Academy, his MSc in Mechanical Engineering from Istanbul Technical University and his PhD in Materials Engineering from Yildiz Technical University. He completed a postdoctoral fellowship at the UIUC. He was an adjunct faculty in the Mechanical Engineering Department at the University of Akron. He

worked in a NASA-funded project. He is currently the head of Mechatronics Engineering Department at Istanbul Gedik University. He is also the director of the Robot Technology Research Application Center.

Batuhan Turgut

Batuhan Turgut, born in 1998, graduated with a bachelor's degree in Mechanical Engineering from Istanbul Gedik University as the top of the department. He started his MSc at Gebze Technical University on wire arc additive manufacturing. He is a candidate IIW Welding Engineer. He is currently working as an R&D Engineer in Gedik Welding

Inc. His main research areas are robotic welding applications and wire arc additive manufacturing.

Mustafa Koçak

Associate Prof. Dr. Mustafa Koçak obtained his PhD (1982) in University of Bath, UK on Fatigue of Aircraft Structures. He was head of department in the GKSS Research Center, Geestacht, Germany between 1984 and 2009. He has chaired IIW Commission X for 9 years between 2003 and 2012. He served as a CEO of the Gedik Holding between 2009 and 2021 and is currently academic member of Istanbul Gedik University and advisor for Gedik Holding.